Quaternary Science Reviews 319 (2023) 108332

Contents lists available at ScienceDirect

Quaternary Science Reviews

journal homepage: www.elsevier.com/locate/quascirev

Glacial Isostatic Adjustment modelling of the mid-Holocene sea-level highstand of Singapore and Southeast Asia

Tanghua Li [a,*], Stephen Chua [a,1], Fangyi Tan [a,b,1], Nicole S. Khan [c], Timothy A. Shaw [a], Jedrzej Majewski [a], Aron J. Meltzner [a,b], Adam D. Switzer [a,b], Patrick Wu [d], Benjamin P. Horton [a,b]

[a] Earth Observatory of Singapore, Nanyang Technological University, Singapore, Singapore
[b] Asian School of the Environment, Nanyang Technological University, Singapore, Singapore
[c] Department of Earth Sciences and the Swire Institute of Marine Science, University of Hong Kong, Hong Kong, China
[d] Department of Geoscience, University of Calgary, Calgary, Alberta, Canada

ARTICLE INFO

Handling Editor: Dr I Hendy

ABSTRACT

The mid-Holocene sea-level highstand refers to higher-than-present relative sea levels (RSLs) in far-field regions between 7000 and 4000 years ago because of equatorial ocean syphoning and continental levering. But the timing, magnitude, and spatial variability of the highstand are uncertain and the highstand parameterization in Glacial Isostatic Adjustment (GIA) modelling is understudied. Here, we use the RSL records of Southeast Asia to investigate the sensitivity of the mid-Holocene highstand properties to Earth and ice model parameters, including lithospheric thickness, mantle viscosity (both 1D and 3D), and deglaciation history of Antarctica and global ice sheets. We found that the Earth model variation only affects the magnitude of the mid-Holocene highstand unless extraordinary low upper mantle viscosity is used. The timing of the highstand moves towards present and there is an absence of the highstand if upper mantle viscosity is $< 4.0 \times 10^{19}$ Pa s or $\leq 1.0 \times 10^{19}$ Pa s, respectively. Ice model variation changes both the timing and magnitude of the mid-Holocene highstand. Delaying the ice-equivalent sea level will shift the timing of the highstand later and result in a lower highstand magnitude. We produced a mid-Holocene highstand "treasure map" that considers topography change and accommodation space to guide future RSL data collection efforts in Southeast Asia. The highstand "treasure map" indicates that the northeast and central west coast of Malay-Thai Peninsula, east coast of Sumatra, north coast of Java, and southwest coast of Borneo are very likely (90% probability) to preserve mid-Holocene highstand evidence.

1. Introduction

The mid-Holocene highstand is a phenomenon where regions distal from polar ice sheets experienced relative sea levels (RSLs) higher than present-day levels between 7000 and 4000 years ago (e.g., Woodroffe and Horton, 2005; Dutton et al., 2015; Kidson, 1982; Mitrovica and Milne, 2002). Mid-Holocene highstands of up to 5 m above present levels have been recorded globally in the Arabian-Persian Gulf (e.g., Al-Mikhlafi et al., 2021; Lokier et al., 2015; Mauz et al., 2022), South America (e.g., Angulo et al., 2006; Fontes et al., 2017; Milne et al., 2005), the Mediterranean (e.g., Mauz et al., 2015; Pirazzoli, 2005) as well as Japan (e.g., Yamano et al., 2019; Yokoyama et al., 2012). However, many of these regions experience significant tectonic deformation that generates additional vertical uncertainties (e.g., Yousefi et al., 2018).

The uncertainty of mid-Holocene highstands (e.g., Chua et al., 2021; Geyh et al., 1979; Horton et al., 2005; Mann et al., 2019; Tan et al., 2023) highlights the need to reconstruct RSL in tectonically stable regions such as Southeast Asia. Except for places near the plate boundaries, Southeast Asia is considered relatively tectonically stable, especially for areas within the Sundaland Core (Hall and Morley, 2004). However the region has spatially and temporally sparse Holocene sea-level data (e.g., Horton et al., 2005; Somboon and Thiramongkol, 1992; Tjia, 1996). Understanding the variability in the timing and magnitude of the mid-Holocene highstand is important for improving Glacial Isostatic Adjustment (GIA) models by constraining the Earth and

* Corresponding author.
E-mail address: li.tanghua@ntu.edu.sg (T. Li).
[1] The authors contributed equally.

https://doi.org/10.1016/j.quascirev.2023.108332
Received 15 June 2023; Received in revised form 20 September 2023; Accepted 22 September 2023
Available online 29 September 2023

ice models.

The mid-Holocene sea-level highstand is caused by two mechanisms that cause a fall in RSL in far-field regions (Fig. 1): (1) equatorial ocean syphoning; and (2) continental levering (Mitrovica and Milne, 2002; Mitrovica and Peltier, 1991; Nakada and Lambeck, 1989). Equatorial ocean syphoning describes the migration of water from far-field regions into areas vacated by forebulge collapse and subsidence at the periphery of deglaciation centers to maintain dynamic equilibrium (e.g., Clark et al., 1978; Mitrovica and Peltier, 1991). Continental levering links to vertical land motion of continental margins due to the increasing ocean loading caused by rising sea levels, which induces a subsidence of offshore regions and an uplift of onshore regions (e.g., Lambeck and Nakada, 1990; Mitrovica and Milne, 2002; Nakada and Lambeck, 1989; Walcott, 1972). Numerical solutions employed to reveal and understand the mid-Holocene sea-level highstand began in the 1970s (e.g., Clark et al., 1978; Lambeck et al., 2003; Mitrovica and Peltier, 1991; Peltier et al., 2022; Walcott, 1972; Yokoyama and Purcell, 2021), but fewer studies have exclusively focused on the mid-Holocene sea-level highstand parameterization in GIA models and improvement of the fit with data (e.g., Bradley et al., 2016; Lambeck, 2002; Mitrovica and Milne, 2002; Yokoyama et al., 2012).

Here, we investigate the sensitivity of the mid-Holocene highstand timing, magnitude and spatial variability to Earth and ice model parameters, including lithospheric thickness, mantle viscosity (both 1D and 3D), deglaciation history of Antarctica, and global deglaciation history. We compare GIA model predictions from two different ice models ICE-6G_C (Argus et al., 2014; Peltier et al., 2015) and ANU-ICE (e.g., Lambeck et al., 2010, 2014, 2017) with a standardized RSL database from Singapore (Chua et al., 2021). The database has a near-complete Holocene record with more than 130 index points that span from ~9.5 ka (thousand years) before present (BP) to present. We identify regions that are sensitive to certain parameters and regions with highstand sensitivity larger than certain thresholds (e.g., Steffen et al., 2014), such as 1.25 m, which is larger than the average vertical uncertainty of mid-Holocene RSL data in Southeast Asia (Chua et al., 2021). To guide future RSL data collection efforts in Southeast Asia, we produce a mid-Holocene highstand "treasure map" that considers topography change and accommodation space to highlight locations of potential highstand record preservation (e.g., Steffen et al., 2014). We validate the highstand "treasure map" with the published records of the highstand from the Southeast Asian region and compare the peak highstand data with peak GIA highstand predictions.

2. Methods

2.1. Glacial Isostatic Idjustment models

The GIA models were computed with 0.5 × 0.5-degree horizontal

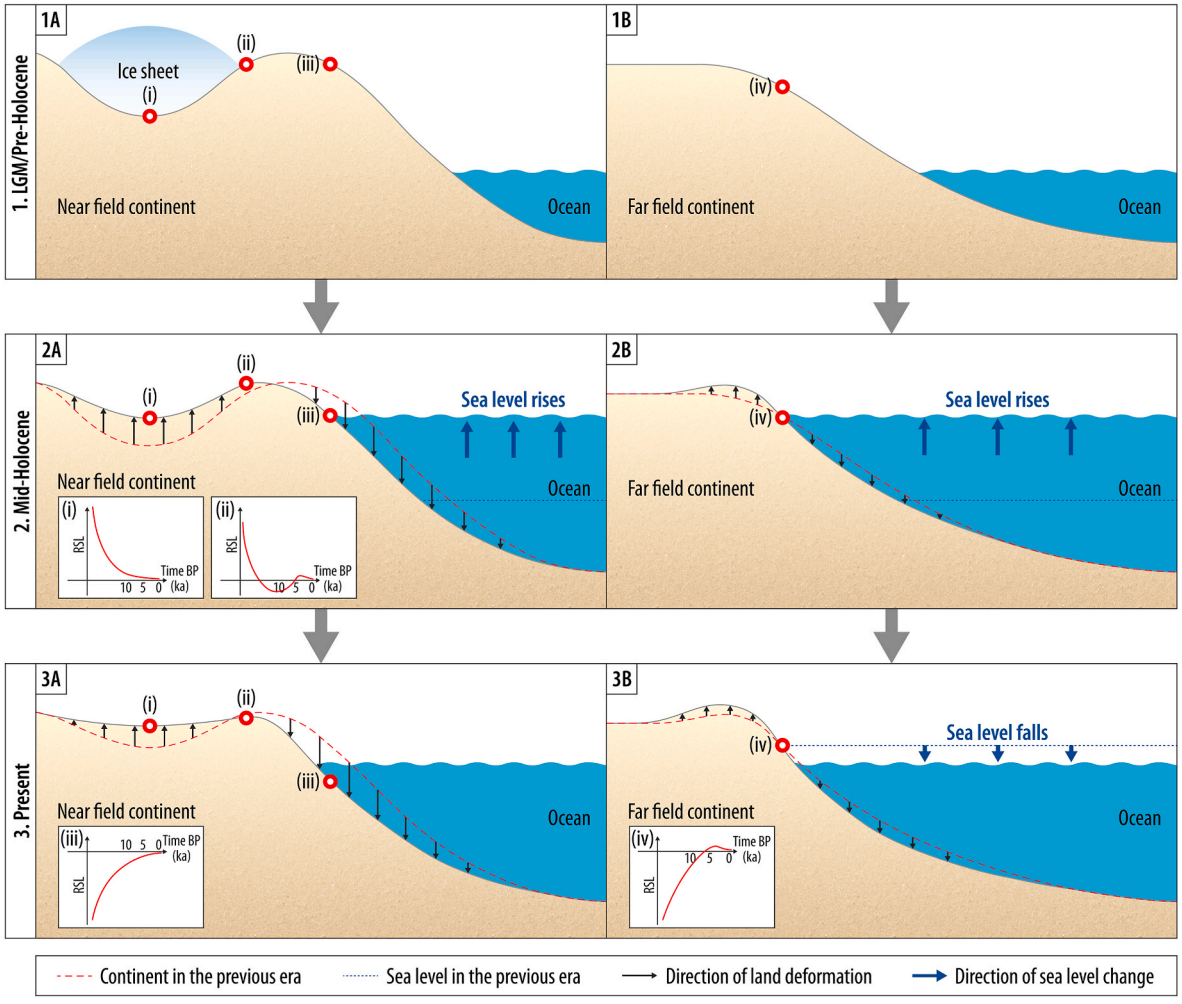

Fig. 1. Schematic of Glacial Isostatic Adjustment process at three stages (Last Glacial Maximum (LGM)/pre-Holocene, mid-Holocene and present), illustrating the equatorial ocean syphoning (panel A) and continental levering (panel B) mechanisms that induce the mid-Holocene sea-level highstand. Insets i-iv demonstrate the sea-level change pattern since LGM till present at locations in (i) near-field close to former ice sheet center (e.g., Hudson Bay, Canada), (ii) near-field close to the former ice sheet margin (e.g., Andoy, Norway), (iii) intermediate-field near the forebulge (e.g., New Jersey, U.S.), (iv) far-field (e.g., Singapore).

resolution near the surface, decreasing with depth to 2.0 × 2.0-degree in the lower mantle to reduce computational resources (Li and Wu, 2019). The model has a temporal resolution of 0.5 ka during the Holocene period (since 12 ka BP) and 1 ka from the Last Glacial Maximum (LGM, 26 ka BP) to 12 ka BP. The GIA models include both the effects of rotational feedback and time-dependent coastlines in the computation of the sea-level equation (Peltier, 1994). The details of the GIA model are described in Li et al. (2022).

We take the ICE-6G_C (VM5a) (Argus et al., 2014; Peltier et al., 2015) as the reference model using the Coupled Laplace-Finite Element method (Wu, 2004). The sensitivity of RSL ($RSL_{Sen}(\theta,\lambda,t)$) to a specific parameter in a GIA model was obtained from the difference between the RSL predictions of the reference model ($RSL_{Ref}(\theta,\lambda,t)$) and a GIA model ($RSL_{Test}(\theta,\lambda,t)$) that allows only one parameter to vary at a time (Fig. 2; Steffen et al., 2014; Wu, 2006), as shown in Equation (1).

$$RSL_{Sen}(\theta,\lambda,t) = RSL_{Test}(\theta,\lambda,t) - RSL_{Ref}(\theta,\lambda,t) \quad (1)$$

Here, θ, λ, and t represent latitude, longitude and time, respectively. For simplicity, we may also use $RSL_{Sen}(t) = RSL_{Test}(t) - RSL_{Ref}(t)$ if we do not refer to any specific location. We investigate the Earth model parameters of lithospheric thickness, 1D and 3D viscosity structures in the upper and lower mantle and ice model parameters of global and Antarctic ice-equivalent sea levels (IESLs).

We test a wide range of Earth parameters that were previously used in GIA modelling studies for the region (e.g., Bradley et al., 2016; Lambeck et al., 2014), including lithospheric thickness varying from 30 to 200 km, 1D upper mantle viscosity varying from 1.0 × 10^{19} to 3.0 × 10^{21} Pa s, and 1D lower mantle viscosity varying from 1.0 × 10^{21} to 1.0 × 10^{24} Pa s. Bradley et al. (2016) suggested that lateral viscosity variations need to be included in the region (e.g., Li et al., 2018; Powell et al., 2021). Therefore, we test the 3D viscosity structures in the upper and lower mantle that were derived from the TX2011 global seismic tomography model (Grand, 2002; Text S1, Fig. S1, S2).

Chua et al. (2021) compared GIA predictions of ICE-6G_C with Holocene RSL data from Southeast Asia. They implied that more ice should melt later than represented in ICE-6G_C during mid-late Holocene, which is likely from Antarctica (Bradley et al., 2016; Tam et al., 2018; Xiong et al., 2020; Yu et al., 2023; Zhang et al., 2021). We, therefore conduct sensitivity tests for models with 1 ka delay of global and Antarctic IESLs to investigate how the highstand in Southeast Asia changes with delayed ice melt.

To test whether the choice of the ice model changes our results significantly, we also conduct sensitivity tests with the ANU-ICE (e.g., Lambeck et al., 2010, 2014, 2017) as the reference ice model while using the same Earth models.

2.2. Mid-Holocene highstand databases for Singapore and Southeast Asia

We use Singapore as a sample site to study the changes in the pattern of RSL predictions and magnitude and timing of the highstand (i.e., maximum positive RSL reached during the Holocene) with the variation of Earth and ice parameters, and how the changes affect the fit with the proxy RSL data. Singapore has numerous quality-controlled RSL data during the Holocene, although a temporal gap does exist during the mid-late Holocene (Fig. 2A; Chua et al., 2021). This paucity of mid-late Holocene RSL data is due to inadequate accommodation space for deposition of intertidal indicators (e.g. Dura et al., 2016) as well as sediment erosion due to modern human activity (e.g., Browning and Sawyer, 2021).

We compiled a mid-Holocene peak highstand database for Southeast Asia (e.g., Geyh et al., 1979; Mann et al., 2023; Meltzner et al., 2017; Somboon and Thiramongkol, 1992; Zhang et al., 2021). We re-evaluated published mid-Holocene (7–4 ka) RSL data following the methodology of the HOLocene SEA-level variability (HOLSEA) working group (Khan et al., 2019). We produced sea-level index points (SLIPs) from sedimentary indicators (e.g., mangrove sediments) and fixed biological indicators (e.g., coral microatolls, oyster belts) that occupy constrained vertical ranges with respect to the tidal frame (i.e., the indicative meaning). To produce a SLIP the indicative meaning of the sea-level indicator must be established. The indicative meaning (Tables S1 and S2) comprises an indicative range, which is the vertical range of the proxy's relationship with tide levels, and a reference water level, or central tendency of the indicative range (Horton et al., 2000; Shennan, 1986; van de Plassche, 1986). A SLIP represents the RSL position at a

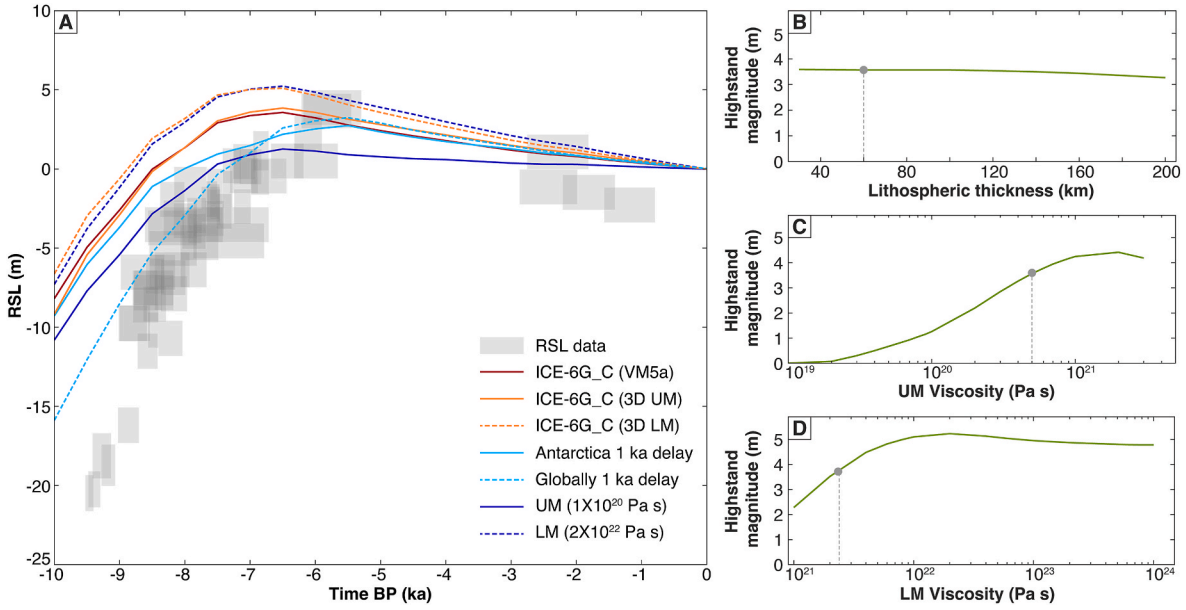

Fig. 2. (A) Reconstructed relative sea-level (RSL) data from Singapore (Chua et al., 2021) compared with RSL predictions of Glacial Isostatic Adjustment (GIA) model ICE-6G_C (VM5a) and other models that are modified from ICE-6G_C (VM5a). The predicted magnitude of the mid-Holocene highstand in GIA models with different (B) lithospheric thicknesses, (C) upper mantle (UM) viscosities, and (D) lower mantle (LM) viscosities fixed with the ICE-6G_C ice model. Grey dots and dashed lines in B, C, D indicate the lithospheric thickness (60 km), upper mantle viscosity (5.0 × 10^{20} Pa s) and (averaged) lower mantle viscosity (~2.6 × 10^{21} Pa s) of VM5a model.

given point in time, with both temporal and vertical uncertainty (Shennan et al., 2015).

Sedimentary and fixed biological indicators that indicate deposition in marine or freshwater environments were used to produce marine (e.g., massive corals, calcareous algal crust, eroded coral microatolls) and terrestrial (e.g., beach ridges) limiting data, which indicate a minimum and maximum bound on RSL, respectively (Shennan et al., 2015).

To calculate RSL, we subtracted the reference water level from the sample elevation, both of which are in the same datum (Shennan and Horton, 2002). All sources of vertical uncertainty associated with determining the elevation of the sample (e.g., levelling uncertainty, tidal uncertainty, indicative range) were added in quadrature to derive the total RSL uncertainty (Shennan and Horton, 2002). For coral microatoll samples whose elevations were reported relative to the elevations of living counterparts (Majewski et al., 2018; Meltzner et al., 2017), the sample elevations are themselves estimates of RSL (Tan et al., 2023).

We calibrated all radiocarbon dates in OxCal 4.4 (Ramsey, 2001) using the latest calibration curves, IntCal20 (Reimer et al., 2020) and Marine20 (Heaton et al., 2020). We obtained the marine reservoir correction (ΔR) by selecting the nearest data source from the Marine20 ΔR database (Reimer and Reimer, 2001), except for data from Meltzner et al. (2017) (Text S2). All U–Th dates in this database were based on the decay constants of Cheng et al. (2013).

We assigned quality ranking to all data points based on the susceptibility of the samples to age and/or elevation errors (Tan et al., 2023). The mid-Holocene peak highstand database is summarized in Table 1 with full citations of the published studies.

2.3. Treasure map of the mid-Holocene highstand data

To guide future mid-Holocene RSL data collection, we produce a mid-Holocene highstand "treasure map" that identifies regions that are likely (67% probability) and very likely (90% probability) to have highstand record preservation. We calculate the mean and standard deviation of RSL predictions from the GIA model ensemble consisting of 45 1D models and two 3D models using the same ice model (ICE-6G_C). Assuming the highstand prediction uncertainties are normally distributed with the mean and standard deviation as calculated from the GIA model ensemble, we estimate the probability distribution of having a highstand during the Holocene period in the region.

The "treasure map" considers the residual between present-day topography ($T_p(\theta,\lambda)$) and accommodation space produced by the predicted highstand elevations (i.e., paleotopography) across Southeast Asia. We identify the regions ($R(\theta,\lambda,t)$) that potentially have highstand record preservation at time t, which were previously below sea level ($T(\theta,\lambda,t) \leq 0$) but now sit above present-day sea level ($T_p(\theta,\lambda) > 0$) as shown in Equation (2).

$$R(\theta,\lambda,t) = \begin{cases} T(\theta,\lambda,t) \leq 0 \\ T_p(\theta,\lambda) > 0 \end{cases} \quad (2)$$

Table 1
Southeast Asia mid-Holocene (7–4 ka BP) sea-level highstand database.

Location	Data No	Lat	Lon	Age (cal yr BP, 2σ)[a]	Material Indicator Type	Highstand RSL (m MSL)	Highstand Uncertainty + (m)	Highstand Uncertainty - (m)	Type	Reference
Thailand										
Chao Phraya Delta	1	13.92	101.58	7578–6194	Basal peat (mangrove)	6.98	1.30	1.30	SLIP	Somboon and Thiramongkol (1992)
Phuket	2	7.75	98.42	6611–6122	Coral	0.17	0.81	0.81	Marine limiting	Scoffin and Le Tissier (1998)
Phang-nga Bay	3	8.19	98.49	5924–5486	Fossil oyster belt	3.50	1.70	1.70	SLIP	Scheffers et al. (2012)
Vietnam										
Southeast Vietnam (Ca Na)	4	11.33	108.83	6776–6423	Beach rock	2.11	0.57	0.57	Marine limiting	Stattegger et al. (2013)
Southeast Vietnam (Ca Na)	5	11.32	108.87	7275–6929	Beach ridge	1.58	0.67	0.67	Terrestrial limiting	Stattegger et al. (2013)
East coast Peninsular Malaysia										
Tioman	6	2.72	104.17	6004–5315	Calcareous algae	1.74	0.97	0.97	Marine limiting	Tjia et al. (1983)
Kuantan	7	3.72	103.27	4817–4098	Back mangrove	1.24	0.15	0.15	SLIP	Hassan (2002)
Kuantan	8	3.70	103.25	4414–4160	Mangrove sediment	1.84	0.45	0.45	SLIP	Zhang et al. (2021)
West coast Peninsular Malaysia										
Kelang (Strait of Malacca)	9	2.99	101.50	6390–5898	Mangrove peat	3.44	0.16	0.15	SLIP	Hassan (2002)
Strait of Malacca	10	1.62	103.42	4862–4097	Mangrove peat	4.88	1.65	1.65	SLIP	Geyh et al. (1979)
Rest of Sunda Shelf										
Singapore	11	1.36	103.69	6270–5330	Upper intertidal deposit	3.94	0.90	0.88	SLIP	Bird et al. (2010)
Belitung	12	−2.70	107.62	6849–6480	Coral microatoll	1.86	0.27	0.27	SLIP	Meltzner et al. (2017)
Natuna Island	13	3.90	108.40	4702–4680	Coral microatoll	0.66	0.29	0.29	SLIP	Wan et al. (2020)
Western Sarawak coast of Borneo	14	2.06	109.65	6087–6037	Coral microatoll	1.65	0.25	0.25	SLIP	Majewski et al. (2018)
Spermonde Archipelago, Makassar Strait	15	−4.95	119.36	6122–5756	Coral microatoll (eroded)	−0.66	0.11	0.11	Marine limiting	Mann et al. (2016)
Pulau Panjang, Java	16	−6.58	110.62	6547–6337	Coral microatoll (eroded)	1.06	0.18	0.18	Marine limiting	Mann et al. (2023)

[a] All 14C ages recalibrated using IntCal20 and Marine20 calibration curves. See methods.

$T_p(\theta,\lambda)$ is the present-day topography from the GEBCO_2022 Grid (Ioc, 2003), which is on a 15 arc-second interval grid. $T(\theta,\lambda,t)$ is the paleo-topography at time t, which is generated following Peltier (2004):

$$T(\theta,\lambda,t) = RSL(\theta,\lambda,t) + \left[T_p(\theta,\lambda) - RSL\left(\theta,\lambda,t_p\right)\right] \quad (3)$$

where $RSL(\theta,\lambda,t_p)$ and $RSL(\theta,\lambda,t)$ are the present-day sea level and sea level at time t, respectively. We combine the $R(\theta,\lambda,t)$ through the whole Holocene period to define $R(\theta,\lambda)$, which is the total area with potential to preserve evidence of the mid-Holocene highstand. The mid-Holocene highstand is determined from the largest residual between the paleo-topography and present-day topography within the Holocene period.

We validate the highstand "treasure map" against the mid-Holocene peak highstand database for Southeast Asia (Table 1) by projecting the peak highstand data locations onto the "treasure map" to confirm the presence of the mid-Holocene highstand preservation in the region. We also compare the peak highstand data with the peak GIA highstand predictions. Although the timing of compiled peak highstand data might be different from that of peak GIA highstand predictions (e.g., 6.5 ka BP with ICE-6G_C), the magnitude of the highstand should be no lower than (i.e., it should be equal to or higher than) the amplitude of the peak highstand data in Table 1 and comparison with peak GIA highstand predictions can validate the GIA model performance.

3. Comparison of GIA model predictions with RSL data from Singapore

The SLIPs from Singapore data show RSL rising rapidly in the early Holocene from ~-21 m at 9.5 ka BP to ~ -4 m at 7.5 ka BP at an average rate of ~8.4 mm/yr (Fig. 2A), which was mainly driven by deglaciation of northern hemisphere Laurentide and Fennoscandia ice sheets in early Holocene (Chua et al., 2021). The RSL predicted by the ICE-6G_C (VM5a) reference model are consistently higher than early Holocene RSL data in Singapore, although the predicted decelerating rate of rise agrees with the data and the misfit magnitude decreases from ~15 m at 9.5 ka BP to ~5 m at 8 ka BP. The predicted RSL curve intersects with the RSL data at ~6 ka BP (Fig. 2A).

The SLIPs in the mid Holocene show the peak RSL highstand of ~3.9 ± 1.1 m at ~6 ka BP or later, driven by equatorial ocean syphoning and continental levering (Figs. 1 and 2A). In contrast, RSL predicted by the ICE-6G_C (VM5a) reference model peaks at 6.5 ka BP with a magnitude of 3.6 m. Following the highstand, the SLIPs data show lower-than-present RSL between 2.5 and 1 ka BP, which has been attributed to local/regional processes (e.g., subsidence, atmosphere-ocean dynamics) (Chua et al., 2021). The predicted RSL declines to present with no lower-than-present RSL prediction because these local/regional processes are not included in GIA modelling (Fig. 2A).

3.1. Sensitivity of the mid-Holocene highstand in Singapore to Earth and ice model parameters

We decreased the upper mantle viscosity from 5.0 × 10^{20} Pa s to 1.0 × 10^{20} Pa s (e.g., Bradley et al., 2016; Lambeck et al., 2014) which lowers: (1) the RSL prediction by ~2.5 m during the early-mid Holocene; and (2) the peak highstand from 3.6 m to 1.3 m at 6.5 ka BP (Fig. 2A). The lowering of RSL is because lower viscosity leads to faster relaxation and lower accumulated magnitude of the highstand.

We increased the lower mantle viscosity from ~2.6 × 10^{21} Pa s (average lower mantle viscosity of VM5a) to 2.0 × 10^{22} Pa s (Horton et al., 2005; Lambeck et al., 2014) which raises: (1) the RSL prediction by ~1.5 m during the early-mid Holocene; and (2) the peak highstand from 3.6 m to 5.2 m at 6.5 ka BP. This is because higher viscosity leads to slower relaxation and larger accumulated magnitude of the highstand.

Incorporating 3D upper mantle viscosity lowers the prediction by ~1 m in the early Holocene and intersects with the prediction of ICE-6G_C (VM5a) at 8 ka BP, while the peak highstand increases slightly to 3.9 m at 6.5 ka BP. Incorporating 3D lower mantle viscosity has a similar effect to increasing the lower mantle viscosity to 2.0 × 10^{22} Pa s with both models intersecting at 7 ka, because the 3D lower mantle mainly shows positive viscosity anomaly (Fig. S1). However, the prediction for the model incorporating 3D lower mantle viscosity is slightly higher by ~0.5 m in early-mid Holocene and lower by ~0.3 m during mid-late Holocene. We should note that the incorporation of 3D viscosity structures in near-field regions (e.g., North America, Europe, Fig. S1, S2) will affect the forebulge evolution (e.g., Roy and Peltier, 2015), consequently influencing the equatorial ocean syphoning and associated highstand characteristics in Southeast Asia (Fig. 1). In all the above instances, changing the Earth model parameters only affects the magnitude of the highstand and does not influence the timing of the highstand.

The highstand magnitude is relatively insensitive to the lithospheric thickness variation (Fig. 2B). Although a thicker lithosphere produces a smaller magnitude of lithospheric flexure and continental levering (Kaufmann et al., 1997; Mitrovica and Milne, 2002; Nakada and Lambeck, 1989), it also produces broader forebulge subsidence that accommodates more water migrating from far-field regions, and the two mechanisms (i.e., equatorial ocean syphoning and continental levering, Fig. 1) contribute comparably in magnitude but opposite in direction to the far-field RSL changes (Mitrovica and Milne, 2002).

With the increase of upper mantle viscosity, the peak highstand magnitude increases and reaches the maximum of 4.4 m with viscosity of 2.0 × 10^{21} Pa s before decreasing (Fig. 2C). We notice a shift in the timing of the peak highstand from 6.5 ka BP towards present when upper mantle viscosity is $< 4.0 \times 10^{19}$ Pa s, and an absence of the highstand when upper mantle viscosity is $\leq 1.0 \times 10^{19}$ Pa s. The latter is because exceptionally low viscosity leads to much faster relaxation, with equilibrium reached by the mid-Holocene, so no deformation exists during the mid-late Holocene to cause the highstand. With an increase of the lower mantle viscosity, the peak highstand increases notably and reaches the maximum of 5.2 m with viscosity of 2.0 × 10^{22} Pa s and then decreases gradually to 4.8 m with viscosity of 1.0 × 10^{24} Pa s (Fig. 2D).

Delay of the global IESL by 1 ka lowers the prediction by ~8 m at 10 ka BP (Fig. 2A). The difference with ICE-6G_C (VM5a) reduces towards the peak highstand, whose timing is shifted by 1 ka from 6.5 ka BP to 5.5 ka BP, with magnitude decreasing to 3.2 m. Similarly, delay of the Antarctic IESL by 1 ka shifts timing of the peak highstand to 5.5 ka BP with magnitude decreasing to 2.7 m. Here, the early Holocene RSL prediction only lowers by ~1 m compared to the ICE-6G_C (VM5a) reference model and the difference increases to ~2 m at 7.5 ka BP, during which the discrepancy between the global IESL (ICE-6G_C) and that with a 1ka delay in the Antarctic component (ICE-6G_C with Antarctica IESL 1 ka delay) is largest (Fig. 3). Unlike changing Earth model parameters, variation of the IESL affects both the magnitude and timing of the highstand. This is because delay of the IESL changes timings of melting slowdown and stop, and shortens the time period for highstand accumulation (Fig. 3).

We infer that for the early-mid Holocene, a decrease of the upper mantle viscosity and delay of IESL improve the model fit with RSL data, while an increase of lower mantle viscosity and incorporation of 3D viscosity in the lower mantle enlarge the misfit. This suggests that the RSL data from Southeast Asia prefer lower viscosities in the upper mantle and a later ending of melting from Antarctica than represented in the ICE-6G_C model (Bradley et al., 2016; Lambeck et al., 2014; Zhang et al., 2021). The sensitivity patterns of the highstand magnitude to upper and lower mantle viscosity variations (Fig. 2C and D) indicate the importance of considering the Earth model uncertainties (Li et al., 2020; Melini and Spada, 2019) and the non-uniqueness of using highstand information to constrain the mid-late Holocene melting histories (Mann et al., 2023; Mitrovica and Peltier, 1991; Nakada and Lambeck, 1989; Nunn and Peltier, 2001; Tan et al., 2023). Because the highstand change due to upper and lower mantle viscosity variation may compensate each other (e.g., a decrease in the upper mantle and an increase in the lower

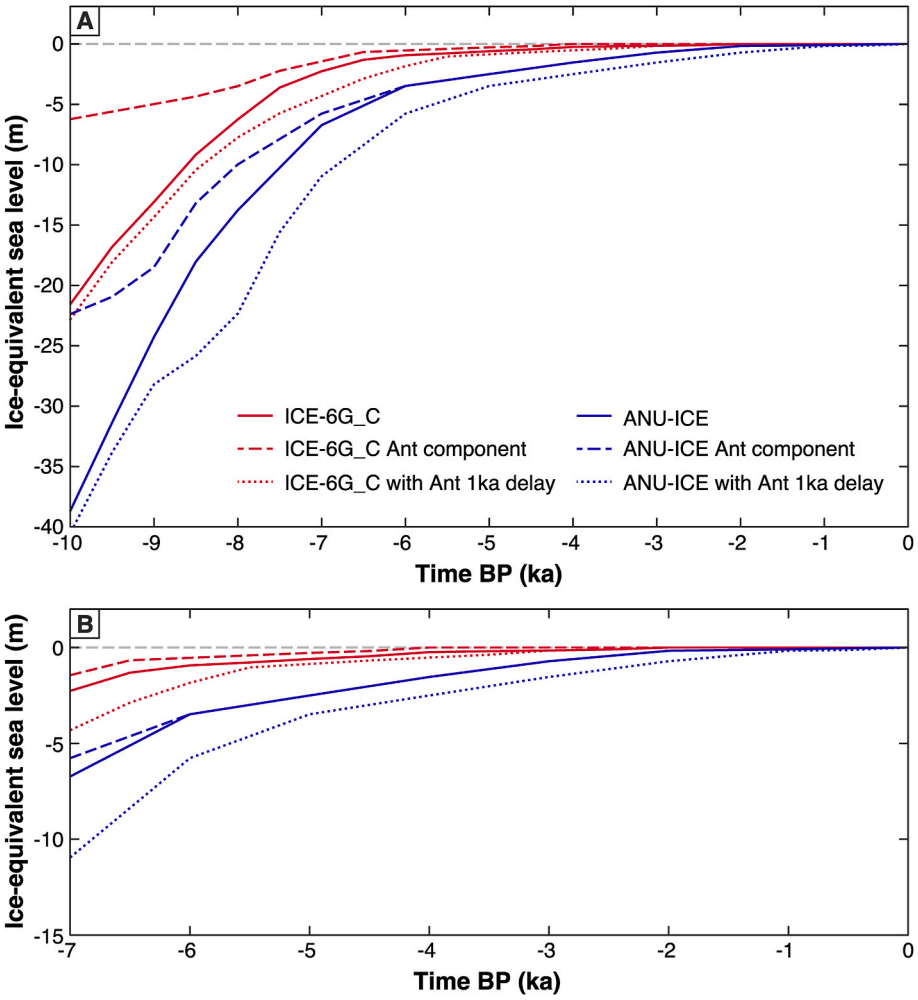

Fig. 3. Ice-equivalent sea-level (IESL, solid lines), its Antarctic component only (dashed lines) and IESL with Antarctic component deglaciation delayed for 1 ka (dotted lines) for ICE-6G_C and ANU-ICE from (A) 10 ka BP and (B) 7 ka BP till present, respectively.

mantle), the confounding effect of the two can further obscure and interact with the melting signal.

4. Mid-Holocene highstand in southeast Asia

The ICE-6G_C (VM5a) model predicted highstand first emerged along the Malacca Strait, east coast of Sumatra and southwest coast of Borneo at ~8.5 ka BP with a magnitude of 0.5–1 m (Fig. 4A and B). The highstand expanded outwards and reached the highest levels (~4.5 m) in Southeast Asia at 6.5 ka BP and decreased afterwards with a consistent highstand distribution pattern (Fig. 4C–G). Hereafter, we focus on the highstand distribution pattern at the peak highstand timing of 6.5 ka BP.

At 6.5 ka BP, highstands existed across all regions of Sundaland and the highstand contours follow the coastlines of outer Sundaland (Fig. 4D). Negative RSLs (RSLs below present) at 6.5 ka BP are found in the South China Sea and Indian Ocean. The pattern of highstand on land and negative RSLs offshore is consistent with the highstand patterns revealed in Australia (Lambeck, 2002), South America (Milne et al., 2005), and previous analyses in the Malay-Thai Peninsula (Horton et al., 2005). Peak highstand magnitudes of over 4 m are estimated for the southern Malacca Strait and along the east coast of Sumatra. The highstand magnitude decreases westwards and southwards and reaches ~0.5 m or less near the northern tip of Aceh and ~2 m along the south coast of central Java, respectively. The highstand is ~3 m along the coast of Borneo and east coast of Malay-Thai Peninsula, ~3.5 along the northern coasts of the Gulf of Thailand and decreases westwards and eastwards. Note that the consistently higher highstand in the west coast compared to the east coast of Malay-Thai Peninsula matches the reconstructed highstand records of Zhang et al. (2021).

4.1. Sensitivity of the mid-Holocene highstand in Southeast Asia to Earth and ice model parameters

A reduction in the upper mantle viscosity from 5.0×10^{20} Pa s to 1.0×10^{20} Pa s decreases the magnitude of RSL at the highstand by > 2 m at 6.5 ka BP around the central Sundaland. Furthermore, the RSL sensitivity decreases outwards going perpendicular to the coastlines and increases to over 2 m in South China Sea (Fig. 5A). The regions with sensitivity ≥ 1.25 m are the coasts of the Gulf of Thailand, Malay-Thai Peninsula, Sumatra (except Aceh), northern Java and Borneo (except northern tip). The RSL sensitivity to an increase in lower mantle viscosity from $\sim 2.6 \times 10^{21}$ Pa s to 2.0×10^{22} Pa s at 6.5 ka BP is distinct from the sensitivity to a decrease in the upper mantle viscosity (Fig. 5A and B), showing more than 2 m of higher RSL centered along the east coast of the Malay-Thai Peninsula. The region with sensitivity ≥ 1.25 m shrinks towards central Sundaland compared with the region with sensitivity ≥ 1.25 m due to a decrease in the upper mantle viscosity.

Incorporation of 3D viscosity structures in the upper and lower mantle both lead to higher RSL at 6.5 ka BP along the east coast of Malay-Thai Peninsula and central west coast of Borneo but with differing magnitudes: over 0.5 m for incorporation of a 3D upper mantle; and over 1.5 m for a 3D lower mantle, respectively (Fig. 5C and D). The

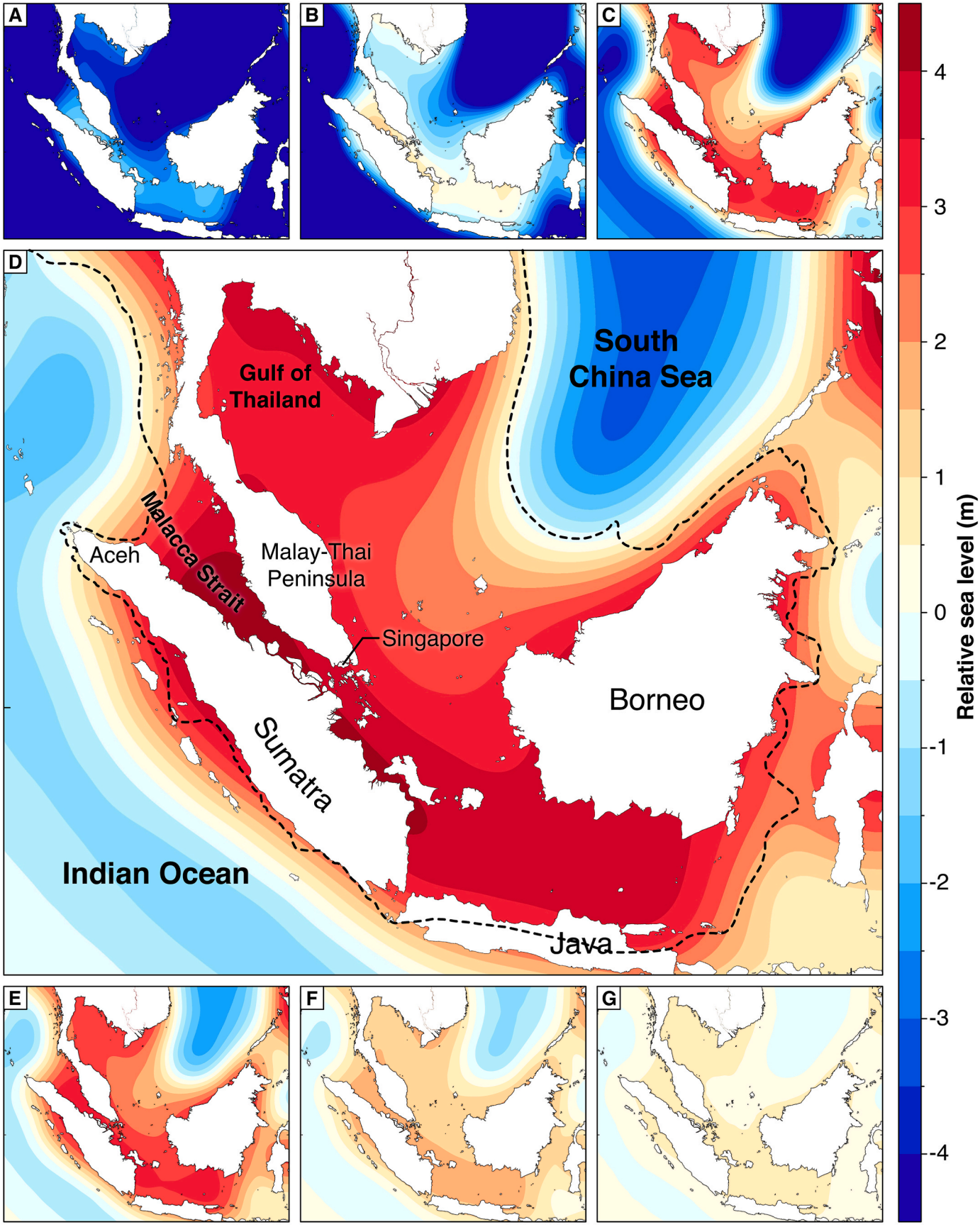

Fig. 4. Relative sea-level (RSL) predictions of Glacial Isostatic Adjustment model ICE-6G_C (VM5a) in Southeast Asia at (A) 9 ka BP, (B) 8.5 ka BP, (C) 7.5 ka BP, (D) 6.5 ka BP, (E) 5.5 ka BP, (F) 3.5 ka BP, and (G) 1.5 ka BP. Positive RSL means above present-day sea level. The dotted line indicates the boundary for Sundaland (Hall, 2013).

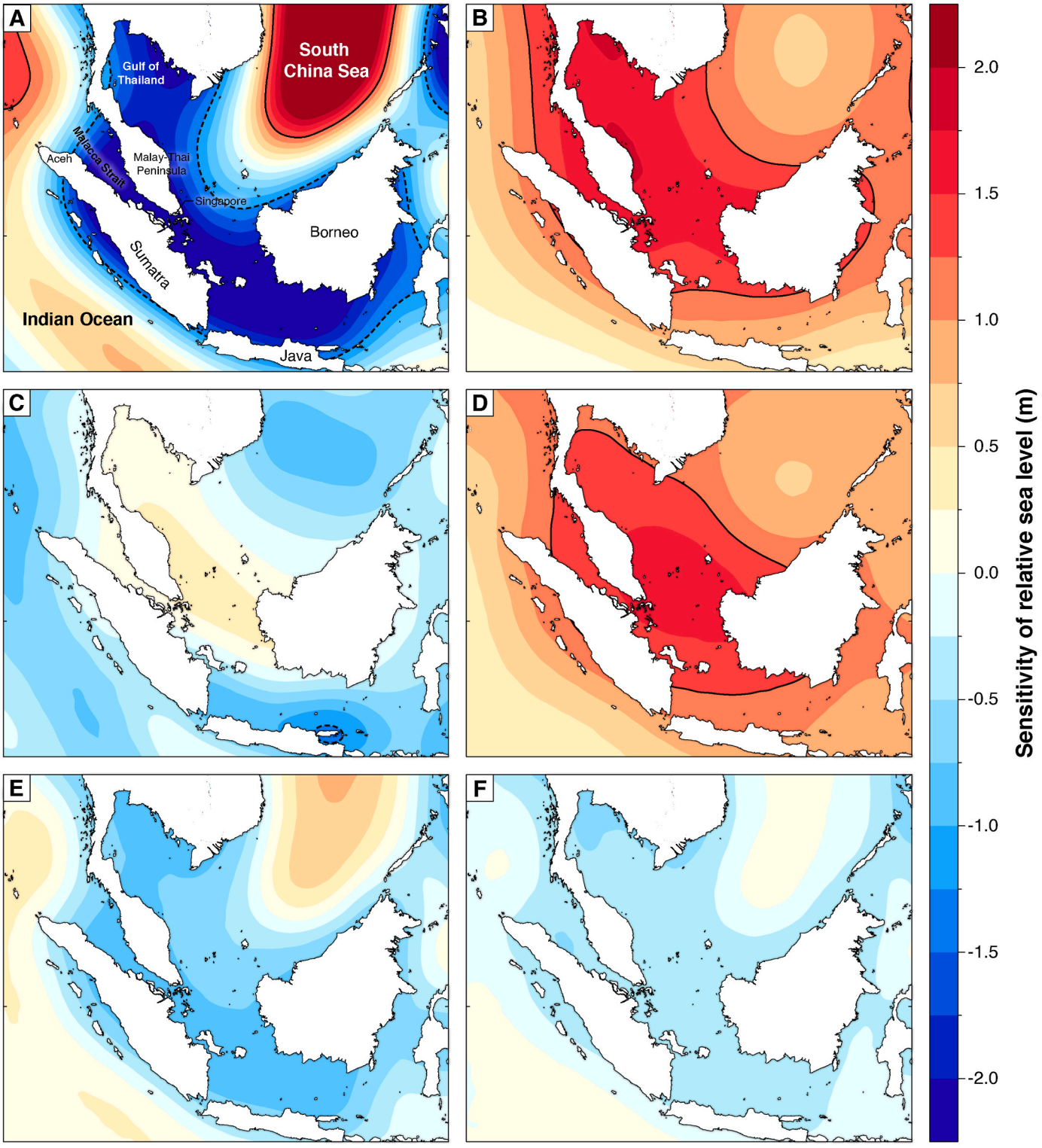

Fig. 5. Relative sea-level (RSL) sensitivity to (A) 1D upper mantle viscosity (1.0×10^{20} Pa s), (B) 1D lower mantle viscosity (2.0×10^{22} Pa s), (C) 3D upper mantle viscosity, (D) 3D lower mantle viscosity at 6.5 ka BP in Southeast Asia. RSL peak highstand sensitivity to 1 ka delay of (E) Antarctic and (F) global ice-equivalent sea-level in Southeast Asia ($RSL_{Test}(5.5) - RSL_{Ref}(6.5)$). The black dashed and solid lines indicate the −1.25 m and 1.25 m contour lines, respectively.

RSL sensitivities decrease going outwards. The region with sensitivity ≥ 1.25 m due to 3D lower mantle (Fig. 5D) further shrinks towards the central Sundaland compared with the sensitivity to 1D lower mantle viscosity increase (Fig. 5B), although the patterns are very similar.

Because the highstand is relatively insensitive to the lithospheric thickness change (Fig. 2B), an increase of the lithospheric thickness from 60 km to 90 km only induces a RSL sensitivity of <0.5 m in magnitude at 6.5 ka BP with negative sensitivity along the coastlines in Southeast Asia (Fig. S3).

We can compare the RSL predictions at the timing of peak highstand of test models with the reference model ICE-6G_C (VM5a) via $RSL_{Test}(5.5) - RSL_{Ref}(6.5)$ (Fig. 5E and F) because shifting the IESL by 1

ka towards the present also changes the timing of the peak highstand by 1 ka (Fig. 2A). RSL peak highstand sensitivities to 1 ka delay of Antarctic and global IESLs show similar pattern of negative sensitivity in the central Sundaland with magnitude of ~1.0 m for the former and of ~0.5 m for the latter (Fig. 5E and F). The shift of the global IESL produces about half the magnitude of the peak highstand sensitivity produced by shifting the Antarctic IESL because only ~50% of the global IESL of ICE-6G_C is from the Antarctic component at 6.5 ka BP (Fig. 3). A later highstand leads to lower highstand magnitude (i.e., negative sensitivity compared with Fig. 4D) attributing to shorter time for the accumulation of the highstand formation using the same Earth model.

The patterns of highstand sensitivity to Earth and ice model parameters in Southeast Asia show some similarities especially in the inner Sundaland, making it challenging to constrain certain parameters via the observational highstand data. More sophisticated techniques on separating RSL contributions from different large ice sheets (e.g., sea-level fingerprinting, Lin et al., 2021) and the spatial gradient among a geographical spread of sea-level data (Kendall et al., 2003; Liu et al., 2016) need to be considered in future studies. Additionally, other types of GIA observational data (e.g., GPS data) from the region need to be included in the inversion process to better constrain GIA input parameters (Mitrovica and Forte, 2004; Peltier et al., 2015; Sasgen et al., 2017).

5. "Treasure map" of the mid-Holocene highstand

The pattern of mean RSL determined from the GIA model ensemble at 6.5 ka BP is very similar to the pattern of RSL at 6.5 ka BP of ICE-6G_C (VM5a). The magnitude of the former is only smaller by ~0.5 m than the latter (Figs. 4D and 6A), because only one parameter is explored in broad range each time and the rest of the parameters are fixed the same as the reference model ICE-6G_C (VM5a). Peak RSL of ~4 m is located along the southern Malacca Strait and east coast of Sumatra, decreasing to the northeast and southwest and reaching ~ -1 m or less in the Indian Ocean and South China Sea (Fig. 6A). The standard deviation of RSL predictions shows similar pattern as the mean RSL at 6.5 ka BP, with much smaller magnitude of ~2 m or less in the inner Sundaland (Fig. 6B).

We assume the highstand prediction uncertainties are normally distributed with the mean and standard deviation as calculated from the GIA model ensemble. Then we identify regions that are likely (67% probability) and very likely (90% probability) to have preserved evidence of a mid-Holocene highstand. The regions that are likely (67% probability) to preserve the highstand record are concentrated near Bangkok, the Mekong River Delta, northeast coast and central west coast of Malay-Thai Peninsula, east coast of Sumatra, north coast of Java, and southwest coast of Borneo (Fig. 7A). The regions that are very likely (90% probability) to have the highstand follow a similar pattern as the likely regions of highstand preservation but with smaller coverage (Fig. 7B). These regions could be key potential areas for future sea-level data collection efforts.

5.1. Validation of the highstand "treasure map"

The compiled peak highstand database is summarized in Table 1 (The HOLSEA template spreadsheet is in the online supplementary material) and overlain on the "treasure map" in Fig. 7A to validate the "treasure map". The locations of highstand records from sedimentary materials (purple dots in Fig. 7A) from Thailand (data No. 1, Table 1), southeast Vietnam (data No. 4, 5), east (data No. 7, 8) and west (data No. 9, 10) coasts of Malay-Thai Peninsula, and Singapore (data No. 11) match well with areas showing highstand preservation denoted in the "treasure map". This validates our assumption that sedimentary material requires time and accommodation space to accumulate (e.g., Dura et al., 2016; Kelsey et al., 2015; Törnqvist et al., 2021) in identified locations in the "treasure map". However, the highstand records (data No. 2–3, 6, 12–16, Table 1) derived from corals, oysters and calcareous algae (green dots in Fig. 7A) do not match the "treasure map" as well as the sedimentary records because these fixed biological indicators do not necessarily need the accommodation space. Kelsey et al. (2015) reconstructed the sea-level history in Aceh, Sumatra and found no evidence of a mid-Holocene sea-level highstand record, which is consistent with our "treasure map" (blue dot in Fig. 7A).

The compiled peak highstand database is compared with the GIA predictions in Fig. 8 to validate the peak GIA highstand predictions. With the exception of the Chao Phraya Delta (Somboon and Thiramongkol, 1992), all peak highstand data are in agreement with peak GIA highstand predictions within 2σ uncertainties, validating the performance of the GIA models (Fig. 8). Chao Phraya Delta has an exceptionally high RSL of 7.0 ± 1.3 m, which is much higher than the rest of the highstand records in Southeast Asia (Table 1) and is higher than the predicted highstand magnitude of 3.6 ± 2.9 m (Fig. 8) and might be due to some unknown local influences.

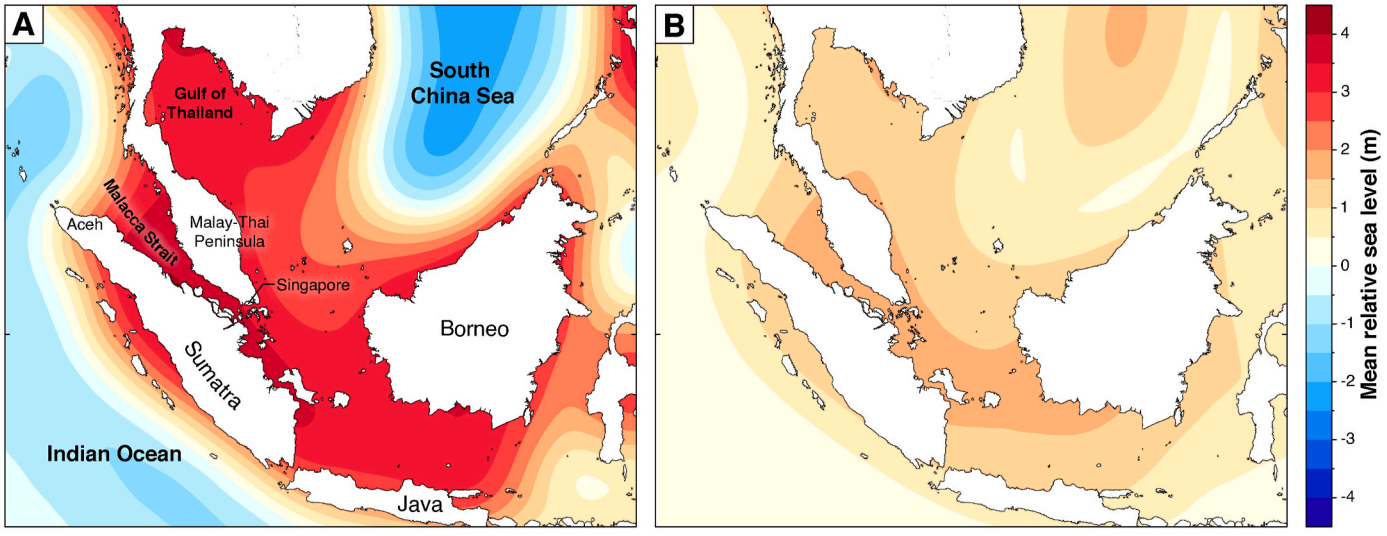

Fig. 6. (A) Mean relative sea level and (B) its standard deviation at 6.5 ka BP in Southeast Asia calculated from the Glacial Isostatic Adjustment model ensemble consisting of 45 1D models and two 3D models with ICE-6G_C ice model. Note that A and B share the same scale.

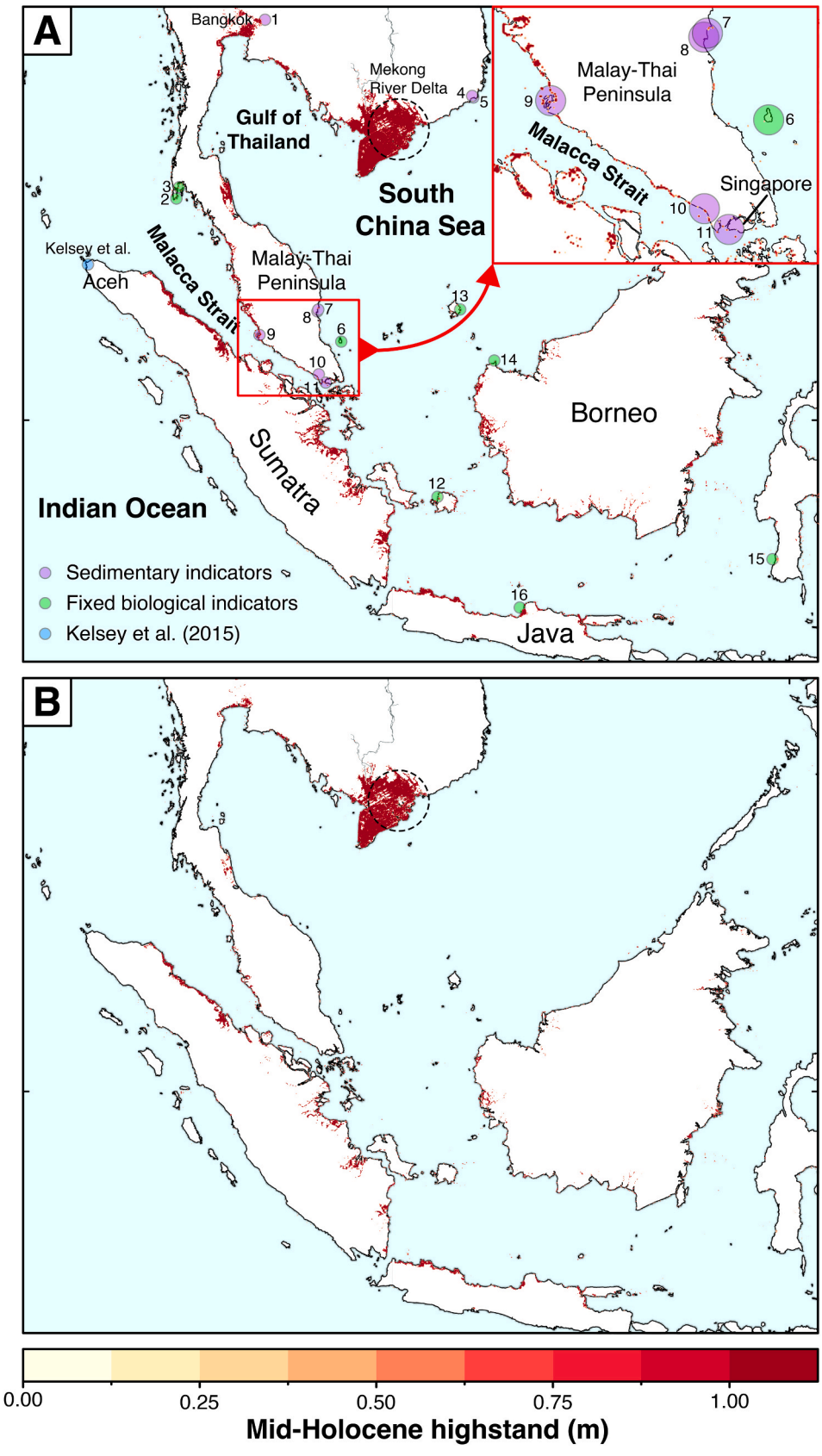

(caption on next page)

Fig. 7. Regions that are (A) likely (67% probability) and (B) very likely (90% probability) to have highstand record preservation considering topography change and accommodation space across Southeast Asia. The legend indicates the predicted highstand magnitude (e.g., dark red dots in A & B indicate the region with predicted highstand magnitude over 1 m; yellow/orange dots indicate the region with predicted highstand magnitude less than 0.5 m, such as parts of northwest coast of Borneo in B). The peak highstand data summarized in Table 1 are shown in purple and green dots for sedimentary materials and fixed biological indicators (e.g., corals, oysters and calcareous algae), respectively. The sea-level reconstruction site in Aceh from Kelsey et al. (2015) showing no evidence of a highstand is shown in blue dot.

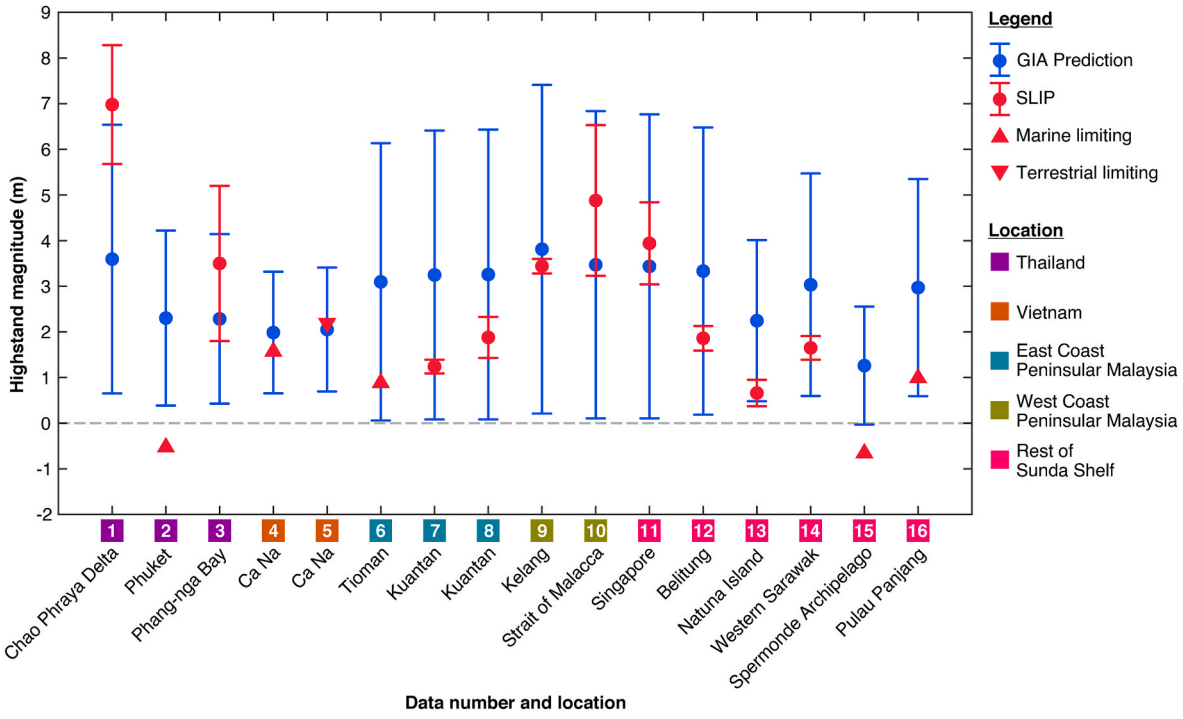

Fig. 8. The mid-Holocene peak highstand data with 2σ relative sea-level (RSL) uncertainties summarized in Table 1 are compared with the peak Glacial Isostatic Adjustment (GIA) highstand predictions with 2σ uncertainties (from the ensemble of 45 1D models and two 3D models as shown in Fig. 6). Note that the limiting data are plotted conservatively. The upwards (downwards) triangle represents the 2σ lower (upper) limit of the RSL uncertainty, indicating that RSL could be anywhere at or above (below) the flat part of the upwards (downwards) triangle. Note that although the timing of peak highstand data points might be different from that of the peak GIA highstand predictions (e.g., 6.5 ka BP with ICE-6G_C), the magnitude of the highstand should be no lower than (i.e., equal or higher than) the peak highstand data shown here.

5.2. *Limitation of the highstand "treasure map"*

Our "treasure map" does not consider the non-GIA regional and local factors that may affect the preservation and elevation of the highstand records, such as tectonics (e.g., Subarya et al., 2006), subsidence (e.g., Sinsakul, 2000), compaction (e.g., Walker et al., 2023), erosion and deposition (e.g., Anthony et al., 2015), and post-depositional change (e.g., Joyse et al., 2023), which all need to be considered for future sea-level reconstructions. For example, the Mekong River Delta is very likely (90% probability) to have the highstand preservation (Fig. 7B), but no SLIPs for the highstand have been obtained. Sea-level records for the Mekong River Delta have been derived only for the early Holocene (Nguyen et al., 2010; Tjallingii et al., 2010) and the late Holocene (4 ka BP - present) (Stattegger et al., 2013). However, the mid-Holocene highstand is largely inferred (e.g., Li et al., 2012) or estimated using limiting data (e.g., Kahlert et al., 2021; Stattegger et al., 2013) due to the lack of mid-Holocene SLIPs. No Holocene sea-level data points exist above modern sea levels (Tjallingii et al., 2014), likely due to the lowering of the Mekong River Delta region due to sediment compaction (Zoccarato et al., 2018). Sediments are also frequently tidally inundated and eroded due to the highly dynamic depositional environment composed of a dense riverine network characterized by significant lateral sediment bar drifts during the late Holocene (Tamura et al., 2012), and exacerbated by human activities in recent years (Anthony et al., 2015).

Similarly, Bangkok sits on the Chao Phraya Delta and experienced significant subsidence in recent years due to sediment compaction due to urbanization, exacerbated by modern groundwater extraction (Sinsakul, 2000). The west coast of Sumatra also experiences significant land-level change due to tectonic deformation along the Sunda megathrust; along the Sumatran outer-arc islands, average interseismic subsidence rates locally ranged from less than 1 mm/yr to more than 12 mm/yr in recent centuries (e.g., Meltzner et al., 2015; Philibosian et al., 2014; Tsang et al., 2015). Thus, any evidence of the highstand may have been removed by coastal processes as the nearshore zone shifts landward due to recent land-level fall.

Although the data from these regions (e.g., Mekong River Delta, Bangkok) may not be ideal for validating GIA models given the large uncertainties in local vertical land motion, comparison of GIA highstand predictions and proxy RSL records from these regions can reveal the local/regional subsidence signal (e.g., King et al., 2021; Liberatore et al., 2022; Wang et al., 2020). For example, Sefton et al. (2022) reconstructed the RSL history on Pohnpei and Kosrae and revealed a ~4.3 m RSL rise over the past ~5.7 ka BP, while the GIA model shows a RSL fall from an over 2.5 m highstand at ~6 ka BP. The discrepancy indicates a mid-late Holocene subsidence of ~1 mm/yr on the two islands.

6. Sensitivity test with the ANU-ICE model

The ANU-ICE (e.g., Lambeck et al., 2010, 2014, 2017) model,

coupled with VM5a Earth model, generates a similar peak highstand pattern as ICE-6G_C (Argus et al., 2014; Peltier et al., 2015) ice model (Fig. 4D, S4), although the ANU-ICE model produces a later timing of peak highstand by ~0.5 ka (6 ka BP) and of ~1 m lower magnitude (~3.5 m along the Malacca Strait). Because the deglaciation history (i.e., IESL) of ANU-ICE decelerates later and ceases later than that of ICE-6G_C (Fig. 3), this leads to shorter time for the accumulation of the highstand formation when coupled with the same Earth model (Argus et al., 2014; Bradley et al., 2016; Lambeck et al., 2014, 2017; Peltier et al., 2015).

Fixing ANU-ICE as the reference ice model, the RSL sensitivities to upper and lower mantle viscosity changes (both 1D and 3D) and shifts of global and Antarctic IESLs in Singapore and Southeast Asia are generally consistent with the sensitivity results of ICE-6G_C (Figs. 2–7, S4-S8). We observe that the ANU-ICE model provides a better fit with the data from Singapore (Fig. S5A) because the global IESL of ANU-ICE was developed to fit RSL data from far-field regions including Singapore (Bird et al., 2007, 2010; Lambeck et al., 2014), while the global IESL of ICE-6G_C is exclusively tuned to fit the tectonically-corrected RSL records from Barbados (Peltier et al., 2015). We also notice the abnormal predicted RSL curve in Singapore from the model with Antarctic IESL shifted 1 ka towards present (cyan solid line in Fig. S5A), which is dominated by its IESL (blue dotted line in Fig. 3). The Antarctic IESL of ICE-6G_C differs significantly from that of ANU-ICE (Fig. 3). The former Antarctic IESL contribution is ~14 m since the LGM and ~12 m since the start of the Holocene, whereas the latter is ~28 m and ~26 m, respectively (Argus et al., 2014; Lambeck et al., 2014, 2017). The much larger Antarctic IESL component in ANU-ICE results in larger RSL sensitivities when shifts of the IESLs were applied (Fig. S6E & F). We are not able to constrain the Antarctica IESL in this study, but more highstand data from the regions we identified (e.g., northeast coast and central west coast of Malay-Thai Peninsula, east coast of Sumatra) can provide better constraints and narrow down the uncertainty of IESL contribution from Antarctica (e.g., Jones et al., 2022).

7. Conclusions

We investigate the mid-Holocene sea-level highstand sensitivities to Earth and ice model parameters in GIA modelling in Singapore and Southeast Asia and compare model predictions with standardized RSL data from Singapore. We test a wide range of Earth model parameters and produce a mid-Holocene highstand "treasure map" considering the topography change and accommodation space to identify regions that may have highstand record preservation, which are validated with a peak highstand database compiled for Southeast Asia. Fixed with the ICE-6G_C ice model, our results show:

1. Earth model variation only affects the magnitude of the mid-Holocene highstand unless extraordinarily low upper mantle viscosity is used (e.g., $< 4.0 \times 10^{19}$ Pa s), which leads to a shift of the timing of the highstand towards present and an absence of the highstand when upper mantle viscosity $\leq 1.0 \times 10^{19}$ Pa s.
2. The magnitude of the mid-Holocene highstand is sensitive to upper mantle viscosity and lower mantle viscosity especially when the lower mantle is $< 1.0 \times 10^{22}$ Pa. In contrast, the mid-Holocene highstand magnitude is relatively insensitive to the lithospheric thickness.
3. Ice model variation can change both the timing and magnitude of the mid-Holocene highstand. Using the same Earth model, delaying the IESL will shift the timing of the highstand later and result in a lower highstand magnitude.
4. The highstand along coasts of inner Sundaland, including west and east coasts of Malay-Thai Peninsula, east coast of Sumatra, and west coast of Borneo, are sensitive to upper (1D) and lower (both 1D and 3D) mantle viscosities.
5. The highstand "treasure map" shows that northeast coast and central west coast of Malay-Thai Peninsula, east coast of Sumatra, north coast of Java, and southwest coast of Borneo are very likely (90% probability) to have the mid-Holocene highstand preservation potential.

Our conclusions are also supported by the ANU-ICE model applying the same group of Earth models, although the ANU-ICE model consistently predicts later timing by ~0.5 ka and lower magnitude by ~1 m of the mid-Holocene highstand, which are largely due to different Antarctic IESLs embedded within the ICE-6G_C and ANU-ICE models (Argus et al., 2014; Lambeck et al., 2014, 2017; Peltier et al., 2015).

Credit author statement

Tanghua Li: Conceptualization, Methodology, Software, Formal analysis, Writing – original draft. Stephen Chua: Data curation, Writing – original draft. Fangyi Tan: Data curation, Writing- Reviewing and Editing. Nicole S. Khan: Conceptualization, Writing- Reviewing and Editing. Timothy A. Shaw: Writing- Reviewing and Editing. Jędrzej Majewski: Data curation, Writing- Reviewing and Editing. Aron J. Meltzner: Writing- Reviewing and Editing. Adam D. Switzer: Writing-Reviewing and Editing. Patrick Wu: Supervision, Writing- Reviewing and Editing. Benjamin P. Horton: Supervision, Funding acquisition, Writing- Reviewing and Editing.

Declaration of competing interest

The authors declare that they have no known competing financial interests or personal relationships that could have appeared to influence the work reported in this paper.

Data availability

Data will be made available on request.

Acknowledgements

We thank W. Richard Peltier for providing the ICE-6G_C ice model and Kurt Lambeck and Anthony Purcell for providing the ANU-ICE ice model. The global ANU-ICE combination model used in this study was kindly provided by Holger Steffen. TL, SC, TAS, AJM and BPH are supported by the Singapore Ministry of Education Academic Research Fund MOE2019-T3-1-004 and MOE-T2EP50120-0007, the National Research Foundation Singapore, and the Singapore Ministry of Education, under the Research Centers of Excellence initiative. AJM is also supported by the National Research Foundation (NRF) Singapore under its NRF Fellowship scheme (Award Number NRF-NRFF11-2019-0008). This research is also supported by the National Research Foundation, Singapore, and National Environment Agency, Singapore under the National Sea Level Programme Funding Initiative (award No. USS-IF-2020-1). Any opinions, findings and conclusions or recommendations expressed in this material are those of the author(s) and do not reflect the views of the National Research Foundation, Singapore and the National Environment Agency, Singapore. This research is conducted in part using the research computing facilities and/or advisory services offered by Information Technology Services, the University of Hong Kong. We express our gratitude to Muhammad Hadi Ikhsan for support with the graphics. This work comprises Earth Observatory of Singapore contribution number 538.

Appendix A. Supplementary data

Supplementary data to this article can be found online at https://doi.org/10.1016/j.quascirev.2023.108332.

References

Al-Mikhlafi, A.S., Hibbert, F.D., Edwards, L.R., Cheng, H., 2021. Holocene relative sea-level changes and coastal evolution along the coastlines of Kamaran Island and As-Salif Peninsula, Yemen, southern Red Sea. Quat. Sci. Rev. 252, 106719.

Angulo, R.J., Lessa, G.C., de Souza, M.C., 2006. A critical review of mid-to late-Holocene sea-level fluctuations on the eastern Brazilian coastline. Quat. Sci. Rev. 25 (5–6), 486–506.

Anthony, E.J., Brunier, G., Besset, M., Goichot, M., Dussouillez, P., Nguyen, V.L., 2015. Linking rapid erosion of the Mekong River delta to human activities. Sci. Rep. 5 (1), 1–12.

Argus, D.F., Peltier, W.R., Drummond, R., Moore, A.W., 2014. The Antarctica component of postglacial rebound model ICE-6G_C (VM5a) based on GPS positioning, exposure age dating of ice thicknesses, and relative sea level histories. Geophys. J. Int. 198 (1), 537–563. https://doi.org/10.1093/gji/ggu140.

Bird, M.I., Austin, W.E.N., Wurster, C.M., Fifield, L.K., Mojtahid, M., Sargeant, C., 2010. Punctuated eustatic sea-level rise in the early mid-Holocene. Geology 38 (9), 803–806.

Bird, M.I., Fifield, L.K., Teh, T.S., Chang, C.H., Shirlaw, N., Lambeck, K., 2007. An inflection in the rate of early mid-Holocene eustatic sea-level rise: a new sea-level curve from Singapore. Estuar. Coast Shelf Sci. 71 (3–4), 523–536.

Bradley, S.L., Milne, G.A., Horton, B.P., Zong, Y., 2016. Modelling sea level data from China and Malay-Thailand to estimate Holocene ice-volume equivalent sea level change. Quat. Sci. Rev. 137, 54–68.

Browning, T.N., Sawyer, D.E., 2021. Vulnerability to watershed erosion and coastal deposition in the tropics. Sci. Rep. 11 (1), 885.

Cheng, H., Edwards, R.L., Shen, C.-C., Polyak, V.J., Asmerom, Y., Woodhead, J., Hellstrom, J., Wang, Y., Kong, X., Spötl, C., 2013. Improvements in 230Th dating, 230Th and 234U half-life values, and U–Th isotopic measurements by multi-collector inductively coupled plasma mass spectrometry. Earth Planet Sci. Lett. 371, 82–91.

Chua, S., Switzer, A.D., Li, T., Chen, H., Christie, M., Shaw, T.A., Khan, N.S., Bird, M.I., Horton, B.P., 2021. A new Holocene sea-level record for Singapore. Holocene 31 (9), 1376–1390.

Clark, J.A., Farrell, W.E., Peltier, W.R., 1978. Global changes in postglacial Sea Level: a numerical calculation 1. Quat. Res. 9 (3), 265–287.

Dura, T., Engelhart, S.E., Vacchi, M., Horton, B.P., Kopp, R.E., Peltier, W.R., Bradley, S., 2016. The role of Holocene relative sea-level change in preserving records of subduction zone earthquakes. Curr. Clim. Change Rep. 2, 86–100.

Dutton, A., Carlson, A.E., Long, Aj, Milne, G.A., Clark, P.U., DeConto, R., Horton, B.P., Rahmstorf, S., Raymo, M.E., 2015. Sea-level rise due to polar ice-sheet mass loss during past warm periods. Science 349 (6244), aaa4019.

Fontes, N.A., Moraes, C.A., Cohen, M.C.L., Alves, I.C.C., França, M.C., Pessenda, L.C.R., Francisquini, M.I., Bendassolli, J.A., Macario, K., Mayle, F., 2017. The impacts of the middle Holocene high sea-level stand and climatic changes on mangroves of the Jucuruçu River, southern Bahia–northeastern Brazil. Radiocarbon 59 (1), 215–230.

Geyh, M.A., Streif, H., Kudrass, H.-R., 1979. Sea-Level changes during the late pleistocene and Holocene in the strait of Malacca. Nature 278 (5703), 441–443.

Grand, S.P., 2002. Mantle shear–wave tomography and the fate of subducted slabs. Philos. Trans. R. Soc. London, Ser. A: Math. Phys. Eng. Sci. 360, 2475–2491. https://doi.org/10.1098/rsta.2002.1077, 1800.

Hall, R., 2013. The palaeogeography of Sundaland and Wallacea since the late Jurassic. J. Limnol. 72.

Hall, R., Morley, C.K., 2004. Sundaland Basins. *Continent-Ocean Interactions within East Asian Marginal Seas*, pp. 55–85.

Hassan, K., 2002. Holocene sea level changes in Peninsular Malaysia. Bull. Geol. Soc. Malays. 45, 301–307.

Heaton, T.J., Köhler, P., Butzin, M., Bard, E., Reimer, R.W., Austin, W.E.N., Ramsey, C.B., Grootes, P.M., Hughen, K.A., Kromer, B., 2020. Marine20—the marine radiocarbon age calibration curve (0–55,000 cal BP). Radiocarbon 62 (4), 779–820.

Horton, B.P., Edwards, R.J., Lloyd, J.M., 2000. Implications of a microfossil-based transfer function in Holocene sea-level studies. Geological Society, London, Special Publications 166 (1), 41–54.

Horton, B.P., Gibbard, P.L., Milne, G.M., Morley, R.J., Purintavaragul, C., Stargardt, J.M., 2005. Holocene sea levels and Peninsula. Southeast Asia 8, 1199–1214.

Ioc, I.H.O., 2003. BODC: Centenary Edition of the GEBCO Digital Atlas, Published on CD-ROM on Behalf of the Intergovernmental Oceanographic Commission and the International Hydrographic Organization as Part of the General Bathymetric Chart of the Oceans, vol. 52. British Oceanographic Data Centre, Liverpool, UK.

Jones, R.S., Johnson, J.S., Lin, Y., Mackintosh, A.N., Sefton, J.P., Smith, J.A., Thomas, E. R., Whitehouse, P.L., 2022. Stability of the Antarctic ice sheet during the pre-industrial Holocene. Nat. Rev. Earth Environ. 3 (8), 500–515.

Joyse, K.M., Khan, N.S., Moyer, R.P., Radabaugh, K.R., Hong, I., Chappel, A.R., Walker, J.S., Sanders, C.J., Engelhart, S.E., Kopp, R.E., 2023. The Characteristics and Preservation Potential of Hurricane Irma's Overwash Deposit in Southern Florida. Marine Geology, USA, 107077.

Kahlert, T., O'Donnell, S., Stimpson, C., Hương, N.T.M., Hill, E., Utting, B., Rabett, R., 2021. Mid-holocene coastline reconstruction from geomorphological sea level indicators in the Tràng an World Heritage site, northern Vietnam. Quat. Sci. Rev. 263, 107001.

Kaufmann, G., Wu, P., Wolf, D., 1997. Some effects of lateral heterogeneities in the upper mantle on postglacial land uplift close to continental margins. Geophys. J. Int. 128 (1), 175–187.

Kelsey, H.M., Engelhart, S.E., Pilarczyk, J.E., Horton, B.P., Rubin, C.M., Daryono, M.R., Ismail, N., Hawkes, A.D., Bernhardt, C.E., Cahill, N., 2015. Accommodation space, relative sea level, and the archiving of paleo-earthquakes along subduction zones. Geology 43 (8), 675–678.

Kendall, R., Mitrovica, J.X., Sabadini, R., 2003. Lithospheric thickness inferred from Australian post-glacial sea-level change: the influence of a ductile crustal zone. Geophys. Res. Lett. 30 (9).

Khan, N.S., Horton, B.P., Engelhart, S., Rovere, A., Vacchi, M., Ashe, E.L., Törnqvist, T.E., Dutton, A., Hijma, M.P., Shennan, I., 2019. Inception of a global atlas of sea levels since the Last Glacial Maximum. Quat. Sci. Rev. 220, 359–371. https://doi.org/10.1016/j.quascirev.2019.07.016.

Kidson, C., 1982. Sea level changes in the Holocene. Quat. Sci. Rev. 1 (2), 121–151.

King, D.J., Newnham, R.M., Gehrels, W.R., Clark, K.J., 2021. Late Holocene sea-level changes and vertical land movements in New Zealand. N. Z. J. Geol. Geophys. 64 (1), 21–36.

Lambeck, K., 2002. Sea level change from mid Holocene to recent time: an Australian example with global implications. Ice Sheets, Sea Level and the Dynamic Earth 29, 33–50.

Lambeck, K., Nakada, M., 1990. Late Pleistocene and Holocene sea-level change along the Australian coast. Palaeogeogr. Palaeoclimatol. Palaeoecol. 89 (1–2), 143–176.

Lambeck, K., Purcell, A., Johnston, P., Nakada, M., Yokoyama, Y., 2003. Water-load definition in the glacio-hydro-isostatic sea-level equation. Quat. Sci. Rev. 22 (2–4), 309–318.

Lambeck, K., Purcell, A., Zhao, J., Svensson, N.-O., 2010. The Scandinavian ice sheet: from MIS 4 to the end of the Last glacial maximum. Boreas 39 (2), 410–435.

Lambeck, K., Purcell, A., Zhao, S., 2017. The North American Late Wisconsin ice sheet and mantle viscosity from glacial rebound analyses. Quat. Sci. Rev. 158, 172–210. https://doi.org/10.1016/j.quascirev.2016.11.033.

Lambeck, K., Rouby, H., Purcell, A., Sun, Y., Sambridge, M., 2014. Sea level and global ice volumes from the Last glacial maximum to the Holocene. Proc. Natl. Acad. Sci. USA 111 (43), 15296–15303. https://doi.org/10.1073/pnas.1411762111.

Li, T., Khan, N.S., Baranskaya, A.V., Shaw, T.A., Peltier, W.R., Stuhne, G.R., Wu, P., Horton, B.P., 2022. Influence of 3D earth structure on glacial isostatic adjustment in the Russian Arctic. J. Geophys. Res. Solid Earth 127 (3), e2021JB023631.

Li, T., Wu, P., 2019. Laterally heterogeneous lithosphere, asthenosphere and sub-lithospheric properties under Laurentia and Fennoscandia from glacial isostatic adjustment. Geophys. J. Int. 216 (3), 1633–1647. https://doi.org/10.1093/gji/ggy475.

Li, T., Wu, P., Steffen, H., Wang, H., 2018. In search of laterally heterogeneous viscosity models of glacial isostatic adjustment with the ICE-6G_C global ice history model. Geophys. J. Int. 214 (2), 1191–1205. https://doi.org/10.1093/gji/ggy181.

Li, T., Wu, P., Wang, H., Steffen, H., Khan, N.S., Engelhart, S.E., Vacchi, M., Shaw, T.A., Peltier, W.R., Horton, B.P., 2020. Uncertainties of glacial isostatic adjustment model predictions in north America associated with 3D structure. Geophys. Res. Lett. https://doi.org/10.1029/2020GL087944 e2020GL087944.

Li, Z., Saito, Y., Mao, L., Tamura, T., Song, B., Zhang, Y., Lu, A., Sieng, S., Li, J., 2012. Mid-Holocene mangrove succession and its response to sea-level change in the upper Mekong River delta, Cambodia. Quat. Res. 78 (2), 386–399.

Liberatore, M., Gliozzi, E., Cipollari, P., Öğretmen, N., Spada, G., Cosentino, D., 2022. Vertical velocity fields along the Eastern Mediterranean coast as revealed by late Holocene sea-level markers. Earth Sci. Rev., 104199

Lin, Y., Hibbert, F.D., Whitehouse, P.L., Woodroffe, S.A., Purcell, A., Shennan, I., Bradley, S.L., 2021. A reconciled solution of Meltwater Pulse 1A sources using sea-level fingerprinting. Nat. Commun. 12 (1), 1–11.

Liu, J., Milne, G.A., Kopp, R.E., Clark, P.U., Shennan, I., 2016. Sea-level constraints on the amplitude and source distribution of Meltwater Pulse 1A. Nat. Geosci. 9 (2), 130–134.

Lokier, S.W., Bateman, M.D., Larkin, N.R., Rye, P., Stewart, J.R., 2015. Late quaternary sea-level changes of the Persian Gulf. Quat. Res. 84 (1), 69–81.

Majewski, J.M., Switzer, A.D., Meltzner, A.J., Parham, P.R., Horton, B.P., Bradley, S.L., Pile, J., Chiang, H.-W., Wang, X., Ng, C.T., Tanzil, J., Müller, M., Mujahid, A., 2018. Holocene relative sea-level records from coral microatolls in Western Borneo, South China Sea. Holocene 28 (9), 1431–1442.

Mann, T., Bender, M., Lorscheid, T., Stocchi, P., Vacchi, M., Switzer, A.D., Rovere, A., 2019. Holocene sea levels in southeast Asia, Maldives, India and Sri Lanka: the SEAMIS database. Quat. Sci. Rev. 219, 112–125.

Mann, T., Rovere, A., Schöne, T., Klicpera, A., Stocchi, P., Lukman, M., Westphal, H., 2016. The magnitude of a mid-Holocene sea-level highstand in the Strait of Makassar. Geomorphology 257, 155–163.

Mann, T., Schöne, T., Kench, P., Lambeck, K., Ashe, E., Kneer, D., Beetham, E., Illigner, J., Rovere, A., Marfai, M.A., 2023. Fossil Java Sea corals record Laurentide ice sheet disappearance. Geology 51 (7), 631–636.

Mauz, B., Ruggieri, G., Spada, G., 2015. Terminal Antarctic melting inferred from a far-field coastal site. Quat. Sci. Rev. 116, 122–132.

Mauz, B., Shen, Z., Alsuwaidi, M., Melini, D., Spada, G., Purkis, S.J., 2022. The mid-Holocene sea-level change in the Arabian Gulf. Holocene 32 (11), 1173–1183.

Melini, D., Spada, G., 2019. Some remarks on glacial isostatic adjustment modelling uncertainties. Geophys. J. Int. 218 (1), 401–413.

Meltzner, A.J., Switzer, A.D., Horton, B.P., Ashe, E., Qiu, Q., Hill, D.F., Bradley, S.L., Kopp, R.E., Hill, E.M., Majewski, J.M., Natawidjaja, D.H., Suwargadi, B.W., 2017. Half-metre sea-level fluctuations on centennial timescales from mid-Holocene corals of Southeast Asia. Nat. Commun. 8, 14387. https://doi.org/10.1038/ncomms14387.

Meltzner, A.J., Sieh, K., Chiang, H.W., Wu, C.C., Tsang, L.L.H., Shen, C.-C., Hill, E.M., Suwargadi, B.W., Natawidjaja, D.H., Philibosian, B., Briggs, R.W., 2015. Time-varying interseismic strain rates and similar seismic ruptures on the Nias–Simeulue patch of the Sunda megathrust. Quat. Sci. Rev. 122, 258–281.

Milne, G.A., Long, A.J., Bassett, S.E., 2005. Modelling Holocene relative seasea-level observations from the Caribbean and South America. Quat. Sci. Rev. 24 (10–11), 1183–1202.

Mitrovica, J.X., Forte, A.M., 2004. A new inference of mantle viscosity based upon joint inversion of convection and glacial isostatic adjustment data. Earth Planet Sci. Lett. 225 (1–2), 177–189.
Mitrovica, J.X., Milne, G.A., 2002. On the origin of late Holocene sea-level highstands within equatorial ocean basins. Quat. Sci. Rev. 21 (20–22), 2179–2190.
Mitrovica, Jerry X., Peltier, W.R., 1991. On postglacial geoid subsidence over the equatorial oceans. J. Geophys. Res. Solid Earth 96 (B12), 20053–20071.
Nakada, M., Lambeck, K., 1989. Late Pleistocene and Holocene sea-level change in the Australian region and mantle rheology. Geophys. J. Int. 96 (3), 497–517.
Nguyen, V.L., Ta, T.K.O., Saito, Y., 2010. Early Holocene initiation of the Mekong River delta, Vietnam, and the response to Holocene sea-level changes detected from DT1 core analyses. Sediment. Geol. 230 (3–4), 146–155.
Nunn, P.D., Peltier, W.R., 2001. Far-field test of the ICE-4G model of global isostatic response to deglaciation using empirical and theoretical Holocene sea-level reconstructions for the Fiji Islands, southwestern Pacific. Quat. Res. 55 (2), 203–214.
Peltier, W.R., 2004. Global glacial isostasy and the surface of the ice-age Earth: the ICE-5G (VM2) model and GRACE. Annu. Rev. Earth Planet Sci. 32, 111–149.
Peltier, W.R., Argus, D.F., Drummond, R., 2015. Space geodesy constrains ice age terminal deglaciation: the global ICE-6G_C (VM5a) model. J. Geophys. Res. Solid Earth 120 (1), 450–487. https://doi.org/10.1002/2014JB011176.
Peltier, W.R., Wu, P.P.-C., Argus, D., Li, T., Velay-Vitow, J., 2022. Glacial isostatic adjustment: physical models and observational constraints. Rep. Prog. Phys. 85 (9), 096801.
Peltier, W Richard, 1994. Ice age paleotopography. Science 265 (5169), 195–201.
Philibosian, B., Sieh, K., Avouac, J.P., Natawidjaja, D.H., Chiang, H.W., Wu, C.C., et al., 2014. Rupture and variable coupling behavior of the Mentawai segment of the Sunda megathrust during the supercycle culmination of 1797 to 1833. J. Geophys. Res. Solid Earth 119 (9), 7258–7287.
Pirazzoli, P.A., 2005. A review of possible eustatic, isostatic and tectonic contributions in eight late-Holocene relative sea-level histories from the Mediterranean area. Quat. Sci. Rev. 24 (18–19), 1989–2001.
Powell, E.M., Pan, L., Hoggard, M.J., Latychev, K., Gomez, N., Austermann, J., Mitrovica, J.X., 2021. The impact of 3-D Earth structure on far-field sea level following interglacial West Antarctic Ice Sheet collapse. Quat. Sci. Rev. 273, 107256.
Ramsey, C.B., 2001. Development of the radiocarbon calibration program. Radiocarbon 43 (2A), 355–363.
Reimer, P.J., Austin, W.E.N., Bard, E., Bayliss, A., Blackwell, P.G., Ramsey, C.B., Butzin, M., Cheng, H., Edwards, R.L., Friedrich, M., 2020. The IntCal20 Northern Hemisphere radiocarbon age calibration curve (0–55 cal kBP). Radiocarbon 62 (4), 725–757.
Reimer, P.J., Reimer, R.W., 2001. A marine reservoir correction database and on-line interface. Radiocarbon 43 (2A), 461–463.
Roy, K., Peltier, W.R., 2015. Glacial isostatic adjustment, relative sea level history and mantle viscosity: reconciling relative sea level model predictions for the US East coast with geological constraints. Geophys. J. Int. 201 (2), 1156–1181.
Sasgen, I., Martín-Español, A., Horvath, A., Klemann, V., Petrie, E.J., Wouters, B., Horwath, M., Pail, R., Bamber, J.L., Clarke, P.J., 2017. Joint inversion estimate of regional glacial isostatic adjustment in Antarctica considering a lateral varying Earth structure (ESA STSE Project REGINA). Geophys. J. Int. 211 (3), 1534–1553.
Scheffers, A., Brill, D., Kelletat, D., Brückner, H., Scheffers, S., Fox, K., 2012. Holocene sea levels along the Andaman Sea coast of Thailand. Holocene 22 (10), 1169–1180.
Scoffin, T.P., Le Tissier, M.D.A., 1998. Late Holocene sea level and reef-flat progradation, Phuket, South Thailand. Coral Reefs 17 (3), 273–276.
Sefton, J.P., Kemp, A.C., Engelhart, S.E., Ellison, J.C., Karegar, M.A., Charley, B., McCoy, M.D., 2022. Implications of anomalous relative sea-level rise for the peopling of Remote Oceania. Proc. Natl. Acad. Sci. USA 119 (52), e2210863119.
Shennan, I., Horton, B.P., 2002. Relative sea-level changes and crustal movements of the UK. J. Quat. Sci. 16 (5–6), 511–526.
Shennan, Ian, 1986. Flandrian sea-level changes in the Fenland. II: Tendencies of sea-level movement, altitudinal changes, and local and regional factors. J. Quat. Sci. 1 (2), 155–179.
Shennan, Ian, Long, A.J., Horton, B.P., 2015. Handbook of Sea-Level Research. John Wiley & Sons.
Sinsakul, S., 2000. Late quaternary geology of the lower central plain, Thailand. J. Asian Earth Sci. 18 (4), 415–426.
Somboon, J.R.P., Thiramongkol, N., 1992. Holocene highstand shoreline of the Chao Phraya delta, Thailand. J. Southeast Asian Earth Sci. 7 (1), 53–60.
Stattegger, K., Tjallingii, R., Saito, Y., Michelli, M., Thanh, N.T., Wetzel, A., 2013. Mid to late Holocene sea-level reconstruction of Southeast Vietnam using beachrock and beach-ridge deposits. Global Planet. Change 110, 214–222.
Steffen, H., Wu, P., Wang, H., 2014. Optimal locations of sea-level indicators in glacial isostatic adjustment investigations. Solid Earth 5 (1), 511.
Subarya, C., Chlieh, M., Prawirodirdjo, L., Avouac, J.-P., Bock, Y., Sieh, K., Meltzner, A. J., Natawidjaja, D.H., McCaffrey, R., 2006. Plate-boundary deformation associated with the great Sumatra–Andaman earthquake. Nature 440 (7080), 46–51.
Tam, C., Zong, Y., Xiong, H., Wu, P., Sun, Y., Huang, G., 2018. A below-the-present late Holocene relative sea level and the glacial isostatic adjustment during the Holocene in the Malay Peninsula. Quat. Sci. Rev. 201, 206–222. https://doi.org/10.1016/j.quascirev.2018.10.009.
Tamura, T., Saito, Y., Nguyen, V.L., Ta, T.K.O., Bateman, M.D., Matsumoto, D., Yamashita, S., 2012. Origin and evolution of interdistributary delta plains; insights from Mekong River delta. Geology 40 (4), 303–306.
Tan, F., Khan, N.S., Li, T., Meltzner, A.J., Majewski, J., Chan, N., Chutcharavan, P.M., Cahill, N., Vacchi, M., Peng, D., 2023. Holocene relative sea-level histories of far-field islands in the mid-Pacific. Quat. Sci. Rev., 107995
Tjallingii, R., Stattegger, K., Stocchi, P., Saito, Y., Wetzel, A., 2014. Rapid flooding of the southern Vietnam shelf during the early to mid-Holocene. J. Quat. Sci. 29 (6), 581–588.
Tjallingii, R., Stattegger, K., Wetzel, A., Van Phach, P., 2010. Infilling and flooding of the Mekong River incised valley during deglacial sea-level rise. Quat. Sci. Rev. 29 (11–12), 1432–1444.
Tjia, H.D., Fujii, S., Kigoshi, K., 1983. Holocene shorelines of Tioman island in the South China sea. Geol. Mijnbouw 62 (4), 599–604.
Tjia, Hong Djin, 1996. Sea-level changes in the tectonically stable Malay-Thai Peninsula. Quat. Int. 31, 95–101.
Törnqvist, T.E., Cahoon, D.R., Morris, J.T., Day, J.W., 2021. Coastal wetland resilience, accelerated sea-level rise, and the importance of timescale. AGU Advances 2 (1), e2020AV000334.
Tsang, L.L.H., Meltzner, A.J., Hill, E.M., Freymueller, J.T., Sieh, K., 2015. A paleogeodetic record of variable interseismic rates and megathrust coupling at Simeulue Island, Sumatra. Geophys. Res. Lett. 42 (24), 10,585–10,594. https://doi.org/10.1002/2015GL066366.
Van de Plassche, O., 1986. Sea-level Research: A Manual for the Collection and Evaluation of Data. Geobooks, Norwich. UK.
Walcott, R.I., 1972. Past sea levels, eustasy and deformation of the earth. Quat. Res. 2 (1), 1–14.
Walker, J.S., Li, T., Shaw, T.A., Cahill, N., Barber, D.C., Brain, M.J., Kopp, R.E., Switzer, A.D., Horton, B.P., 2023. A 5000-year record of relative sea-level change in New Jersey, USA. The Holocene 33 (2), 167–180.
Wan, J.X.W., Meltzner, A.J., Switzer, A.D., Lin, K., Wang, X., Bradley, S.L., Natawidjaja, D.H., Suwargadi, B.W., Horton, B.P., 2020. Relative sea-level stability and the radiocarbon marine reservoir correction at Natuna Island, Indonesia, since 6400 yr BP. Mar. Geol. 430, 106342.
Wang, F., Zong, Y., Mauz, B., Li, J., Fang, J., Tian, L., Chen, Y., Shang, Z., Jiang, X., Spada, G., 2020. Holocene sea-level change on the central coast of Bohai Bay, China. Earth Surf. Dyn. 8 (3), 679–693.
Woodroffe, S.A., Horton, B.P., 2005. Holocene sea-level changes in the Indo-Pacific. J. Asian Earth Sci. 25 (1), 29–43.
Wu, P., 2004. Using commercial finite element packages for the study of earth deformations, sea levels and the state of stress. Geophys. J. Int. 158 (2), 401–408.
Wu, P., 2006. Sensitivity of relative sea levels and crustal velocities in Laurentide to radial and lateral viscosity variations in the mantle. Geophys. J. Int. 165 (2), 401–413. https://doi.org/10.1111/j.1365-246X.2006.02960.x.
Xiong, H., Zong, Y., Li, T., Long, T., Huang, G., 2020. Coastal GIA processes revealed by the early to middle Holocene sea- level history of east China. Quat. Sci. Rev. 233, 106249 https://doi.org/10.1016/j.quascirev.2020.106249.
Yamano, H., Inoue, T., Adachi, H., Tsukaya, K., Adachi, R., Baba, S., 2019. Holocene sea-level change and evolution of a mixed coral reef and mangrove system at Iriomote Island, southwest Japan. Estuar. Coast Shelf Sci. 220, 166–175.
Yokoyama, Y., Okuno, J., Miyairi, Y., Obrochta, S., Demboya, N., Makino, Y., Kawahata, H., 2012. Holocene sea-level change and Antarctic melting history derived from geological observations and geophysical modeling along the Shimokita Peninsula, northern Japan. Geophys. Res. Lett. 39 (13).
Yokoyama, Y., Purcell, A., 2021. On the geophysical processes impacting palaeo-sea-level observations. Geoscience Letters 8 (1), 1–19.
Yousefi, M., Milne, G.A., Love, R., Tarasov, L., 2018. Glacial isostatic adjustment along the Pacific coast of central North America. Quat. Sci. Rev. 193, 288–311.
Yu, F., Li, N., Tian, G., Huang, Z., Xiong, H., Li, T., Liu, S., Liu, Y., 2023. A re-evaluation of Holocene relative sea-level change along the Fujian coast, southeastern China. Palaeogeogr. Palaeoclimatol. Palaeoecol., 111577
Zhang, Y., Zong, Y., Xiong, H., Li, T., Fu, S., Huang, G., Zheng, Z., 2021. The middle-to-late Holocene relative sea-level history, highstand and levering effect on the east coast of Malay Peninsula. Global Planet. Change 196, 103369.
Zoccarato, C., Minderhoud, P.S.J., Teatini, P., 2018. The role of sedimentation and natural compaction in a prograding delta: insights from the mega Mekong delta, Vietnam. Sci. Rep. 8 (1), 1–12.